Detailed analysis of the $3d^{-1}\rightarrow 4p\,\pi^{-2}$ normal Auger spectra in HBr and DBr

R. Püttner,[1] Y. F. Hu,[2] G. M. Bancroft,[2] H. Aksela,[1] E. Nõmmiste,[1]* J. Karvonen,[1] A. Kivimäki,[1] and S. Aksela[1]

[1]*Department of Physical Sciences, University of Oulu, PL 3000, 90401 Oulu, Finland*
[2]*Department of Chemistry, The University of Western Ontario, London, Ontario, Canada N6A 5B7*

(Received 1 December 1998)

High-resolution Br MVV Auger spectra of HBr and DBr have been recorded using monochromatized synchrotron radiation. We present a detailed analysis and reassignment of the spectra in the $3d^{-1}\rightarrow 4p\,\pi^{-2}$ region. This part of the spectra exhibits the spin-orbit and ligand-field splitting of the $3d^{-1}$ core-hole states and a vibrational structure of the final states influenced by vibrational lifetime interference. The equilibrium distances and the vibrational energies of the final states $^1\Sigma^+$, $^1\Delta$, and $^3\Sigma^-$ are derived from the intensity distribution of the vibrational substates. From the shape of the peaks identified as transitions to the $^3\Sigma^-$ state a splitting of $\cong 50$ meV between the components $^3\Sigma_0^-$ and $^3\Sigma_1^-$ is concluded. Agreement between the experimental spectra and fitted results for both HBr and DBr is very satisfactory. [S1050-2947(99)08406-1]

PACS number(s): 33.80.Eh, 33.20.Tp, 33.15.Dj

I. INTRODUCTION

During the last two decades a number of effects in normal-Auger spectra have been resolved. Although the two-hole final states populated subsequent to core ionization are normally dissociative and lead to broad spectral features, in some cases, the final states are stable with respect to dissociation; consequently, they possess discrete vibrational levels and are, therefore, of high experimental and theoretical interest. First observations of vibrational fine structure in Auger spectra were reported in N_2 by Siegbahn *et al.* [1] and in CO by Correira *et al.* [2]. For CO it was shown that vibrational lifetime interference influences the observed line shape [2]. Later on, vibrational lifetime interference was used by Carroll *et al.* to explain the line shape of some features in the KVV Auger spectra of, e.g., NO [3].

In the late eighties Karlsson *et al.* examined the Auger spectra subsequent to shallow core ionization in HCl/DCl (Cl $2p^{-1}$) [4], HBr/DBr (Br $3d^{-1}$) [5], and HI (I $4d^{-1}$) [6]. The final-state configurations with two holes in the nonbonding π valence orbital, π^{-2}, are of particular interest, since the Auger transitions to these states show a number of narrow lines. In all these molecules, the π^{-2} final-state configuration is split into the electronic states $^1\Sigma^+$, $^1\Delta$, and $^3\Sigma^-$ (see, e.g., Fig. 1). Some structures in these Auger spectra were identified as transitions to vibrational substates [4,5] on the basis of isotopic shifts; all structures were assigned accordingly. In the early 1990s, ligand-field splitting was resolved in the spin-orbit split $4d$ and $3d$ photoelectron lines of HI and HBr, respectively [7,8]. Since in the two-step model, i.e., by regarding photoionization and Auger transition separately, the intermediate state of the entire process, namely, the core-hole state, can be considered as the ''initial'' state for the Auger transition, ligand-field splitting had to be considered in the analyses of the Auger spectra of HBr and HI. For HI the resulting reassignment lead to a debate in

literature [6,7,9]. However, the situation is similar in HBr/DBr. We show that ligand-field splitting of the core-hole states and the vibrational splitting of the final states are of the same order of magnitude ($\cong 200$ meV) and have comparable influence on the normal-Auger spectra hindering a straightforward analysis.

In this investigation, we have recorded the high-resolution MVV Auger spectra of HBr and DBr using monochromatized synchrotron radiation. We show that for Auger transitions to final states with quasistable potential-energy curves, ligand-field splitting of the intermediate state as well as vibrational splitting, including lifetime interference, have to be considered to obtain reliable interpretations of the spectra. In addition, we show that the influence of vibrational lifetime interference, although well known since the eighties, has been underestimated in the analysis of normal-Auger spectra. In detail, we determine the equilibrium distances and vibrational energies as well as the energetic splittings of the final
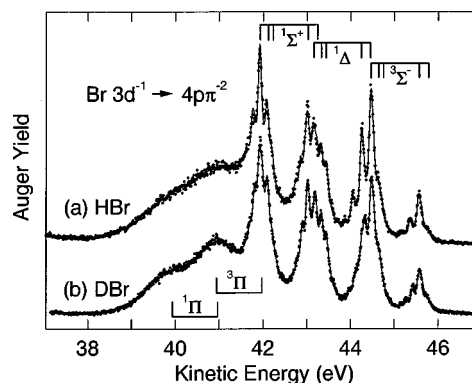
FIG. 1. Overview spectrum of the $3d^{-1}\rightarrow 4p\,\pi^{-2}$ Auger transitions of HBr (upper part) and DBr (lower part). The energy positions of the $v''=0\rightarrow v'=0$ transitions to the final states $^1\Sigma^+$, $^1\Delta$, and $^3\Sigma^-$ are given by the upper vertical-bar diagrams indicating the five ligand-field components of the intermediate state. The lower vertical-bar diagrams indicate the energies of the $4p\sigma^{-1}4p\pi^{-1}$ ($^{3,1}\Pi$) final states. The solid line through the data points represents the fitted results.

states. From the broadening of the peaks identified as transitions to the $^3\Sigma^-$ state, we conclude a spin-orbit splitting of $\cong 50$ meV between the $^3\Sigma_0^-$ and $^3\Sigma_1^-$ components.

II. EXPERIMENT

The measurements were performed at the gas-phase beamline 51 [10,11] (The Finnish Beamline) at the MAX I storage ring in Lund, Sweden. The beamline uses radiation from a short-period undulator and includes a modified SX700 plane-grating monocromator. A rotatable high-resolution spectrometer Scienta 200 was used as an electron analyzer [12]. The Auger spectra of the present studies were obtained at the pseudomagic angle of $54.7°$. The spectrum of HBr (DBr) was measured using a broad photon band at the photon energy of 102 eV (93 eV). The analyser pass energy was 10 eV (20 eV) resulting in an experimental resolution of 20 meV (30 meV). The observed linewidths were, therefore, mostly determined by the lifetime width of the Br $3d^{-1}$ states of 95 meV [13]. The kinetic energies of the Auger electrons were calibrated using the $N_{4,5}OO$ lines in xenon.

III. DATA ANALYSIS

The spin-orbit and ligand-field splittings and vibrational excitations observed in the Br $3d^{-1}$ photoelectron spectrum of HBr demonstrate the presence of a substantial number of different intermediate states contributing to the normal-Auger spectra. From recent photoelectron spectra, the ligand-field splittings between the $3d_{5/2}^{-1}(^2\Delta_{5/2})$ and the

$3d_{5/2}^{-1}(^2\Pi_{3/2})$, $3d_{5/2}^{-1}(^2\Sigma_{1/2})$, $3d_{3/2}^{-1}(^2\Delta_{3/2})$, $3d_{3/2}^{-1}(^2\Pi_{1/2})$ states were extracted to be 175(2) meV, 286(4) meV, 1087(2) meV, 1300(1) meV, respectively [8,14]. Additionally, the spectra showed vibrational substates with a splitting of $\hbar\omega \cong 315$ meV and a $v''=1$-to-$v''=0$ intensity ratio of $\cong 0.05$ [14]. The value for the lifetime width of $\Gamma=95$ meV is taken from photoabsorption spectra [13].

Since the spacing between the different intermediate states is of the same order as the lifetime width Γ, interference becomes important. The Auger process can then be described by [2]

$$I(E)\propto\sum_f\left|\sum_n\frac{\langle\Psi_f|Q|\Psi_n\rangle\langle\Psi_n|D|\Psi_i\rangle}{E-(E_n-E_f)+i\Gamma/2}\right|^2, \quad (1)$$

where Ψ denotes the total molecular wave function, Q the Coulomb operator, D the dipole operator, E the energy as well as i, n (m), and f the intitial, intermediate, and final states, respectively. By applying the adiabatic approximation, i.e., the separability of the electronic and vibrational motions, the total molecular wave functions can be written as $|\Psi_f\rangle=|\psi_\varphi\rangle|\varphi'\rangle$, $|\Psi_n\rangle=|\psi_\nu\rangle|\nu'\rangle$, $|\Psi_m\rangle=|\psi_\mu\rangle|\mu'\rangle$, and $|\Psi_i\rangle=|\psi_i\rangle|i'\rangle$. $|\psi_\alpha\rangle$ represents the electronic part and $|\alpha'\rangle$ the vibrational part of the total molecular wave function. By using $D_\nu=\langle\psi_\nu|D|\psi_i\rangle$ and $Q_{\nu\varphi}=\langle\psi_\varphi|Q|\psi_\nu\rangle$ as well as suppressing the photoelectron degrees of freedom [post-collision interaction (PCI)—their influence will be discussed below], Eq. (1) can be written as

$$I(E)\propto\sum_\varphi\sum_{\varphi'}\sum_\nu\sum_{\nu'}\frac{|Q_{\nu\varphi}|^2|D_\nu|^2|\langle\varphi'|\nu'\rangle|^2|\langle\nu'|i'\rangle|^2}{[E-(E_{\nu\nu'}-E_{\varphi\varphi'})]^2+\Gamma^2/4}$$

$$+\sum_\varphi\sum_{\varphi'}\sum_\nu\sum_{\mu'\neq\nu'}\frac{|Q_{\nu\varphi}|^2|D_\nu|^2\langle\varphi'|\nu'\rangle\langle\nu'|i'\rangle\langle i'|\mu'\rangle\langle\mu'|\varphi'\rangle\{[E-(\epsilon_{\nu\nu'}^{\varphi\varphi'})][E-(\epsilon_{\nu\mu'}^{\varphi\varphi'})]+\Gamma^2/4\}}{\{[E-(\epsilon_{\nu\nu'}^{\varphi\varphi'})][E-(\epsilon_{\nu\mu'}^{\varphi\varphi'})]+\Gamma^2/4\}^2+(E_{\nu\nu'}-E_{\nu\mu'})^2\Gamma^2/4}$$

$$+\sum_\varphi\sum_{\varphi'}\sum_{\mu\neq\nu}\sum_{\nu'}\frac{Q_{\nu\varphi}Q_{\mu\varphi}^*D_\nu D_\mu^*|\langle\varphi'|\nu'\rangle|^2|\langle\nu'|i'\rangle|^2\{[E-(\epsilon_{\nu\nu'}^{\varphi\varphi'})][E-(\epsilon_{\mu\nu'}^{\varphi\varphi'})]+\Gamma^2/4\}}{\{[E-(\epsilon_{\nu\nu'}^{\varphi\varphi'})][E-(\epsilon_{\mu\nu'}^{\varphi\varphi'})]+\Gamma^2/4\}^2+(E_{\nu\nu'}-E_{\mu\nu'})^2\Gamma^2/4}$$

$$+\sum_\varphi\sum_{\varphi'}\sum_{\mu\neq\nu}\sum_{\mu'\neq\nu'}\frac{Q_{\nu\varphi}Q_{\mu\varphi}^*D_\nu D_\mu^*\langle\varphi'|\nu'\rangle\langle\nu'|i'\rangle\langle i'|\mu'\rangle\langle\mu'|\varphi'\rangle\{[E-(\epsilon_{\nu\nu'}^{\varphi\varphi'})][E-(\epsilon_{\mu\mu'}^{\varphi\varphi'})]+\Gamma^2/4\}}{\{[E-(\epsilon_{\nu\nu'}^{\varphi\varphi'})][E-(\epsilon_{\mu\mu'}^{\varphi\varphi'})]+\Gamma^2/4\}^2+(E_{\nu\nu'}-E_{\mu\mu'})^2\Gamma^2/4}, \quad (2)$$

with $\epsilon_{\nu\mu'}^{\varphi\varphi'}=E_{\nu\mu'}-E_{\varphi\varphi'}$. The first term is the direct term that is used in the two-step model for Auger decay, the second term describes the vibrational lifetime interference, the third term the electronic-state lifetime interference, and the last term describes interferences between different vibrational states of different electronic states.

In the present paper the $3d^{-1}\rightarrow4p\pi^{-2}$ Auger spectra of HBr and DBr were treated with a least-squares fit analysis. We included the direct term and the vibrational lifetime interference term of Eq. (2), however, we neglected the last two terms (see below). As a consequence of the adiabatic

approximation, the intensity of a transition to one final state characterized by its electronic and vibrational quantum numbers can be given in Eq. (2) as a product of the electronic and vibrational matrix elements. The electronic, namely, the dipole and Coulomb matrix elements, are identical for HBr and DBr allowing us to describe them with the same set of parameters. The vibrational matrix elements were calculated on the basis of potential-energy surfaces of the states, which were assumed to be equal for HBr and DBr in the space of the real distances r and, therefore, could be described in this space by using only one set of parameters for both molecules. To realize identical parameters for HBr and DBr,

both spectra were fitted simultaneously. This allows us to describe both spectra with approximately 30 parameters.

For the calculation of the vibrational matrix elements, Morse potentials for the ground state, the intermediate $3d^{-1}$ core-hole state, and the $4p\pi^{-2}$ final states were assumed; possible differences in the potential-energy surfaces for the ligand-field components of the $3d^{-1}$ core-hole state were neglected. The values for the potential-energy surfaces of the ground state and the $3d^{-1}$ state were taken from literature [15] and recent photoelectron spectra [14], respectively. The calculations of the vibrational matrix elements are not performed in the real space, but in the space of the normal coordinates. Since the transformation from the real space to the normal coordinates is different due to the different reduced masses $\mu_{H,D}$, differences in the vibrational fine structure for HBr and DBr are observed. In the space of the normal coordinates, the Morse potential can be described with the equilibrium distance q, the vibrational energy $\hbar\omega$, and the anharmonicity $x\hbar\omega$. To ensure the assumption of identical potential-energy surfaces in the real space r, the potential-energy surfaces of HBr and DBr are described by one set of q, $\hbar\omega$, and $x\hbar\omega$ and the fixed ratios $q_H = \sqrt{(\mu_H/\mu_D)}\ q_D$, $\hbar\omega_H = \sqrt{(\mu_H/\mu_D)}\hbar\omega_D$, and $x\hbar\omega_H = (\mu_H/\mu_D)x\hbar\omega_D$. Using these values as the fit parameters, the wave functions and matrix elements were calculated in each iteration. An algorithm based on the publications of Halman and Laulich [16] and Ory *et al.* [17] was used to calculate the wave function and the matrix elements.

In the derivation of Eq. (2) from Eq. (1), the photoelectron degrees of freedom have been suppressed. The photoelectron degrees of freedom, however, embed the PCI effect through relaxation of photoelectron wave functions. The present analysis shows that PCI is evident in the spectra. By including the photoelectron degrees of freedom in the derivation of Eq. (2), this equation becomes more complicated: The direct terms can be approximated by a Kuchiev and Sheinerman line shape, which is used in the present paper in its simplified form given by Armen *et al.* [18]. For the less important cross terms, we use the line shape given by the corresponding terms of Eq. (2) by including an average energy shift to approximate the photoelectron relaxation; this shift amounts to 10 meV (20 meV) for the HBr (DBr) spectrum measured at $h\nu = 102$ eV ($h\nu = 93$ eV). All line shapes are convoluted with a Gaussian of 20 meV (30 meV) full width at half maximum for HBr (DBr) to simulate the resolution of the electron analyzer.

In the present analysis, we included the direct terms and the vibrational lifetime interference terms. Since one can expect that the last two terms are of the same order of magnitude as the vibrational lifetime interference terms, there is no reason to neglect these terms, but it would be substantially more complicated to take these terms into account: From our analysis we are able to obtain the sign of the vibrational matrix elements directly; however, there is no direct access to D_ν and Q_ν. In principle, $|D_\nu|^2$ could be obtained from the photoelectron spectra and $|Q_\nu|^2$ in an approximate way from fitting the Auger spectra, i.e., $Q_{\nu\varphi}Q^*_{\mu\varphi}D_\nu D^*_\mu$ could be estimated regardless of its sign. Consequently, for a correct description of the electronic-state lifetime interference of each term $Q_{\nu\varphi}Q^*_{\mu\varphi}D_\nu D^*_\mu$, an additional discrete parameter with the allowed values $+1$ and -1 has to be included,
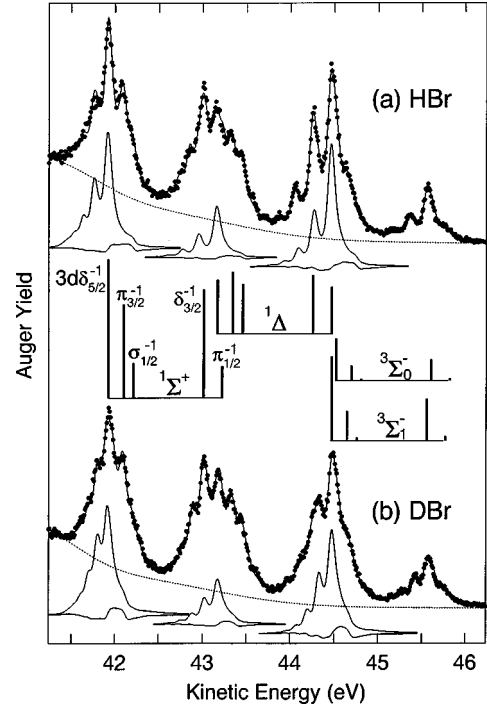
FIG. 2. The spectrum of the $3d^{-1} \rightarrow 4p\pi^{-2}$ Auger transitions in detail. The upper part (a) shows HBr and the lower part (b) DBr. The solid line through the data points represents the fitted result. The upper solid subspectra in each spectrum show the vibrational fine structure of the transitions to the final states, represented by the $3d_{5/2}^{-1}(^2\Delta_{5/2}) \rightarrow {}^1\Sigma^+$, ${}^1\Delta$, and ${}^3\Sigma^-$ transitions. The lower lines show the contributions of the vibrational lifetime interference terms. In these subspectra the splitting of the ${}^3\Sigma^-$ final state is neglected. The dotted lines represent the background. The vertical-bar diagrams between the spectra represent the energy positions and intensities of the different transitions to the final states caused by ligand-field spitting of the intermediate $3d^{-1}$ state.

leading for HBr/DBr to a strong increase of the number of fit parameters.

IV. RESULTS AND DISCUSSION

Figure 1 displays the overview spectra of the $3d^{-1} \rightarrow 4p\pi^{-2}$ normal-Auger transitions of HBr and DBr. They overlap with the broad and dissociative $4p\pi^{-1}4p\sigma^{-1}(^{1,3}\Pi)$ final states. The $4p\pi^{-2}$ configuration is threefold split into ${}^1\Sigma^+$, ${}^1\Delta$, and ${}^3\Sigma^-$. Five transitions to each of these final states (see top of diagram) indicate a splitting of the $3d^{-1}$ core-hole state due to the ligand field; each of the transitions exhibit a rich vibrational structure due to changes in the equilibrium distance between the core-excited and final states. The positions of the $v''=0 \rightarrow v'=0$ transitions from the different ligand-field components of the intermediate state to the final states ${}^1\Sigma^+$, ${}^1\Delta$, and ${}^3\Sigma^-$ are also indicated with vertical-bar diagrams. In the present paper v'' (v') indicates the vibrational substates in the $3d^{-1}$ core-hole state (final state). Note that in this figure the splitting of the ${}^3\Sigma^-$ state into ${}^3\Sigma_0^-$ and ${}^3\Sigma_1^-$ is neglected. The solid line through the data points represents the fitted result. There is, in general, a good agreement between experiment and fit for both HBr and DBr, as shown in more detail in Figs. 2–6.

In the upper (lower) part of Fig. 2, the Auger transitions
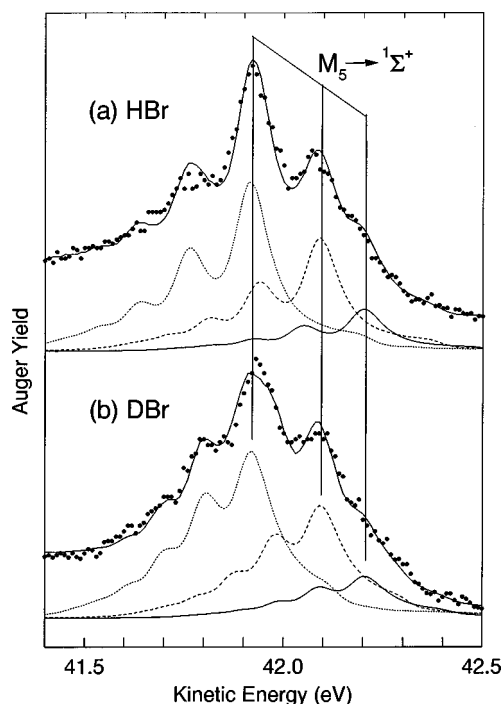
FIG. 3. Detailed spectrum for the energy region from 41.4 eV to 42.5 eV including the $M_5 \rightarrow {}^1\Sigma^+$ transitions. The solid line through the data points represents the fitted result. The vibrational fine structure of the $3d_{5/2}^{-1}(^2\Delta_{5/2}) \rightarrow {}^1\Sigma^+$, $3d_{5/2}^{-1}(^2\Pi_{3/2}) \rightarrow {}^1\Sigma^+$, and $3d_{5/2}^{-1}(^2\Sigma_{1/2}) \rightarrow {}^1\Sigma^+$ transitions is given by the dotted, dashed, and solid subspectra, respectively. The vertical lines indicate the $v''=0 \rightarrow v'=0$ transitions.
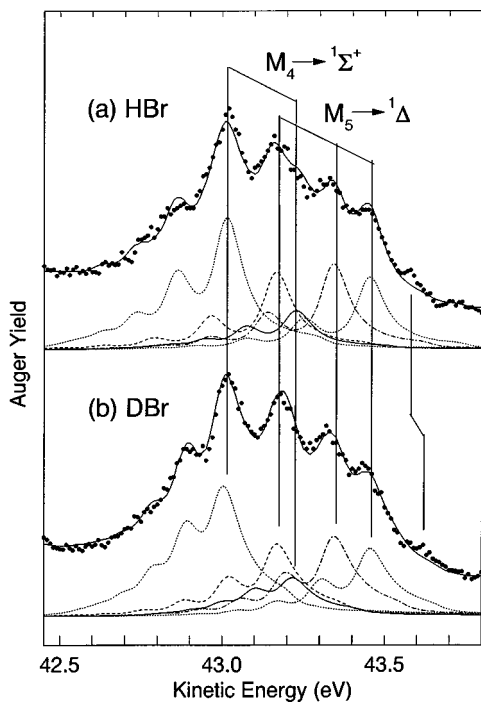
FIG. 4. Detailed spectrum for the energy region from 42.45 eV to 43.80 eV including the $M_4 \rightarrow {}^1\Sigma^+$ and $M_5 \rightarrow {}^1\Delta$ transitions. The solid line through the data points represents the fitted result. The vibrational fine structure of the final states is given by the subspectra. The vertical lines indicate the $v''=0 \rightarrow v'=0$ transitions.
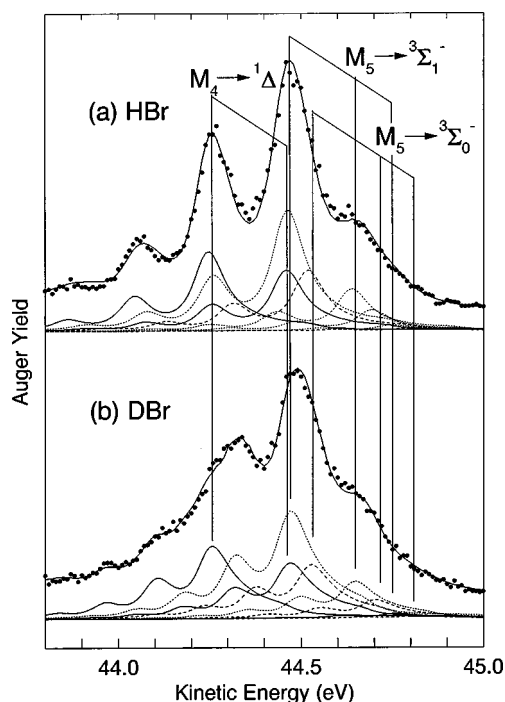
FIG. 5. Detailed spectrum for the energy region from 43.8 eV to 45.0 eV including the $M_4 \rightarrow {}^1\Delta$ and $M_5 \rightarrow {}^3\Sigma^-$ transitions. The solid line through the data points represents the fitted result. The vibrational fine structure of the $M_4 \rightarrow {}^1\Delta$, $M_5 \rightarrow {}^3\Sigma_1^-$, and $M_5 \rightarrow {}^3\Sigma_0^-$ transitions are given by the solid, dotted, and dashed subspectra, respectively. The vertical lines indicate the $v''=0 \rightarrow v'=0$ transitions.

to the $4p\pi^{-2}$ configuration of HBr (DBr) are shown in more detail. From the minima of the potential-energy surfaces between the states ${}^3\Sigma_0^-$ and ${}^3\Sigma_1^-$, ${}^1\Delta$, ${}^1\Sigma^+$, the energy differences between these states are derived to be 55(10) meV, 1359(10) meV, and 2624(10) meV, respectively. The values agree well with the results of 48 meV, 1465 meV, and 2697 meV from recent fully relativistic configuration interaction calculations by Matila *et al.* [19]. These theoretical results confirm, in particular, the derived value for the spin-orbit splitting of the ${}^3\Sigma^-$ state. The vibrational fine structure of the $3d_{5/2}^{-1}(^2\Delta_{5/2}) \rightarrow 4p\pi^{-2}$ transition is given for all final states in the upper subspectra for both HBr and DBr. Note that for all transitions leading to one particular final state, the vibrational structure is equal due to the assumption of equal potential-energy surfaces for the intermediate state. The lower subspectra for both HBr and DBr indicate the contributions of vibrational lifetime interference, which are significant for the high-energy side of each vibrational band, in particular for DBr (see below).

The influence of the ligand-field splitting from the $3d^{-1}$ intermediate state for both HBr and DBr is shown in the middle of the Fig. 2. The intensities for the Auger transitions starting from different ligand-field components of the intermediate state are given by the vertical-bar diagrams. Each transition leading to one particular final state in HBr (DBr) is split by the same vibrational fine structure as shown in the upper subspectra of the top (bottom) part of Fig. 2. Due to a slight line broadening of the transitions to the ${}^3\Sigma^-$ state, a splitting into ${}^3\Sigma_0^-$ and ${}^3\Sigma_1^-$ occurs as indicated. In the analysis, the intensity ratio for the transitions to the ${}^3\Sigma_0^-$ and ${}^3\Sigma_1^-$
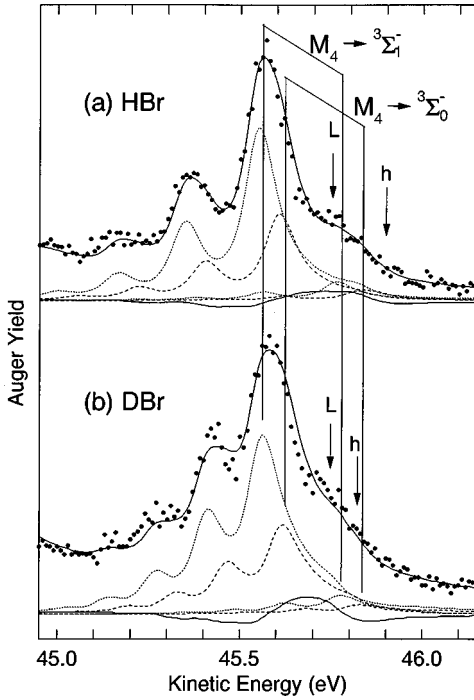
FIG. 6. Detailed spectrum for the energy region from 44.95 eV to 46.15 eV including the $M_4 \rightarrow {}^3\Sigma^-$ transitions. The solid subspectrum represents the fitted result, and the dotted (dashed) subspectra the ${}^3\Sigma_1^-$ (${}^3\Sigma_0^-$) final states. The solid subspectrum represents vibrational lifetime interference contributions summarized over all final states. ''h'' indicates the expected positions of the $v''=1 \rightarrow v'=0$ transitions and ''L,'' the energy position of the strongest vibrational lifetime interference contributions for the $3d_{3/2}^{-1}({}^2\Delta_{3/2}) \rightarrow {}^3\Sigma^-$ states.

states is fixed to the ratio of the number of magnetic substates, i.e., 1:2. For the corresponding Auger transition to the ${}^3P_0$ and ${}^3P_1$ states in Kr, it is observed that the intensity ratio depends on the spin-orbit component of the intermediate state [20]. We can thus expect different ${}^3\Sigma_0^-$-to-${}^3\Sigma_1^-$ intensity ratios for transitions starting from different ligand-field components of the Br $3d^{-1}$ intermediate state. However, the quality of the spectra does not allow us to investigate this intensity ratio in detail.

The intensities of the Auger transitions starting from the five ligand-field components are very different for the ${}^1\Sigma^+$ and ${}^3\Sigma_{0,1}^-$ states, in contrast to the similar photoelectron intensities [8,13]. For the ${}^1\Sigma^+$ and ${}^3\Sigma_{0,1}^-$ states, the decrease in intensity from $3d_{5/2}^{-1}({}^2\Delta_{5/2})$ to $3d_{5/2}^{-1}({}^2\Pi_{3/2})$ to $3d_{5/2}^{-1}({}^2\Sigma_{1/2})$ as well as from $3d_{3/2}^{-1}({}^2\Delta_{3/2})$ to $3d_{3/2}^{-1}({}^2\Pi_{1/2})$ can be understood qualitatively using similar overlap arguments as applied for H_2S by Svensson *et al.* [21]. An intense Auger transition is expected for a large spatial overlap between the core-ionized and final states. The final-state π orbitals are located perpendicular to the molecular axis. As a consequence, the highest Auger intensity can be expected from core-hole states that have a spatial orientation perpendicular to the molecular axis. According to Johnson *et al.* [22], the $3d_{5/2}^{-1}({}^2\Delta_{5/2})$ state can be described with $3d_{xy}$ and $3d_{x^2-y^2}$ atomic orbitals, which are perpendicular to the molecular axis. The $3d_{3/2}^{-1}({}^2\Delta_{3/2})$ and $3d_{5/2}^{-1}({}^2\Pi_{3/2})$ states are described as a linear combination of the $3d_{xy}/3d_{x^2-y^2}$ and $3d_{xz}/3d_{yz}$ atomic orbitals. The latter pair of atomic orbitals has an orientation of 45° with respect to the molecular axis. The states $3d_{5/2}^{-1}({}^2\Sigma_{1/2})$ and $3d_{3/2}^{-1}({}^2\Pi_{1/2})$ can be described by a linear combination of the $3d_{xz}/3d_{yz}$ atomic orbital and the $3d_{z^2}$ atomic orbital, which is in the molecular axis. The highest intensity is, therefore, expected for the $3d_{5/2}^{-1}({}^2\Delta_{5/2}) \rightarrow 4p\pi^{-2}$ Auger transitions and the lowest for the $3d_{5/2}^{-1}({}^2\Sigma_{1/2})$ and $3d_{3/2}^{-1}({}^2\Pi_{1/2}) \rightarrow 4p\pi^{-2}$ Auger transitions. However, for the ${}^1\Delta$ final state, the intensities for the different transitions due to the ligand-field splitting of the intermediate state are almost similar. This behavior is not understood, but due to the large number of strongly overlapping Auger transitions in this part of the spectrum, the error bars of the intensities have to be considered larger than for the other parts of the spectra.

From the subspectra in Fig. 2 it can be seen that the vibrational side bands for the transitions to the ${}^1\Delta$ and ${}^3\Sigma^-$ states are very similar, and considerably different from the vibrational structure for the transitions to the ${}^1\Sigma$ state. This difference is reflected in the equilibrium distances, vibrational energies, and anharmonicities summarized in Table I. The experimental vibrational energies and the equilibrium distances are very similar for the ${}^1\Delta$ and ${}^3\Sigma^-$ states. In contrast to this, the obtained equilibrium distance is larger and the vibrational energy smaller for the ${}^1\Sigma^+$ state. For comparison, the theoretical results obtained by Banichevich *et al.* [23] and Matila *et al.* [19] are also given. This comparison of the experimental results with the calculations shows that the values for the ${}^1\Delta$ and ${}^3\Sigma^-$ states agree well

TABLE I. Results of the fit analysis. Given are the equilibrium distances r, the vibrational energies $\hbar\omega$, and anharmonicities $x\hbar\omega$ for HBr in the ground state, the core-excited state, and the final states ${}^1\Sigma^+$, ${}^1\Delta$, and ${}^3\Sigma^-$. The vibrational energies (anharmonicities) of DBr are smaller by the factor of 0.711 (0.506). For comparison, the results of the nonrelativistic (NR) and relativistic (R) calculations of Ref. [23] as well as of the multireference configuration interaction (MRCI) Dirac-Fock calculations of Ref. [19] are given. The experimental values for the ground state and the $3d^{-1}$ state are taken from Refs. [15] and [14], respectively.

	r (Å)				$\hbar\omega$ (meV)				$x\hbar\omega$ (meV)	
	expt.	NR [23]	R [23]	MRCI [19]	expt.	NR [23]	R [23]	MRCI [19]	expt.	MRCI [19]
Ground state	1.413	1.41	–	1.413	328.2	358.3	–	333	5.6	4.8
$3d^{-1}$	1.450(3)	–	–	1.445	315(5)	–	–	–	–	–
${}^3\Sigma^-$	1.563(4)	1.55	1.49	1.542	218(3)	232	248	235	8.8(1.0)	8.7
${}^1\Delta$	1.560(4)	1.54	1.49	1.541	220(3)	242	248	240	9.9(1.0)	11.6
${}^1\Sigma^+$	1.581(4)	1.55	1.50	1.559	177(5)	241	250	–	13.0(2.0)	–

with the nonrelativistic calculations. The agreement between the experimental and theoretical values for the $^1\Sigma^+$ state is, however, significantly worse [23]. The results of the relativistic calculations in Ref. [23] disagrees considerably more for all states. The recent theoretical results of the multireference configuration interaction (MRCI) Dirac-Fock calculations of Matila *et al.* [19] reveal an excellent agreement between experiment and theory; in particular, these calculations describe correctly the tendencies in the equilibrium distances of the final states $^3\Sigma^-$, $^1\Delta$, and $^1\Sigma^+$. Matila *et al.* explain the larger equilibrium distance and smaller vibrational energy of the $^1\Sigma^+$ state as compared to the $^1\Delta$ and $^3\Sigma^-$ states by an avoided level crossing of the $^1\Sigma_0^+$ and $^3\Pi_0$ states [19].

Figures 3 to 6 display the results of the fit analysis in detail and reveal the complexity of the spectra. The similarity of the Auger spectra of HBr and DBr is due to the facts that (i) for all Auger transitions the $v''=0 \to v'=0$ transition is the most intense one and (ii) the ligand-field and vibrational splittings are comparable ($\cong 150-250$ meV). It is interesting to note that the spectra of HBr and DBr in Figs. 3 and 4 are very similar, because the spectra are dominated by ligand-field splitting. In contrast, the spectra of HBr and DBr in Figs. 5 and 6 are noticably different since vibrational contributions are more important.

In the low kinetic-energy regions of Figs. 3 and 4 it can be observed that in HBr the linewidths of the transitions to the $^1\Sigma^+$ final state including higher vibrational substates v' are slightly larger than the used value for the lifetime of the core-excited states. We assume that this is caused by the avoided level crossing of the states $^1\Sigma_0^+$ and $^3\Pi_0$ leading to (i) a shallower potential well and an increased rate of dissociation caused by tunneling through the potential barrier or (ii) contributions beyond the adiabatic approximation. A detailed theoretical study of these effects will be given in Ref. [19]. In the higher-energy region of Fig. 4 at $\cong 43.5$ eV a spectral feature can be seen which shifts upon deuteration and is only partially described by the fitted result. Due to the observed shift, we assign these spectral features as higher vibrational substates of the $3d_{3/2}^{-1}(^2\Delta_{3/2}) \to {}^1\Delta$ transition and conclude that the applied Morse potential does not correctly describe the intensities of the higher vibrational substates.

Figure 6 shows the fits of the $M_4 \to {}^3\Sigma^-$ transitions of HBr and DBr and displays the influence of the vibrational lifetime interference. The expected energy position of the $3d_{3/2}^{-1}(^2\Delta_{3/2})$ $v''=1 \to {}^3\Sigma^- v'=0$ transition is indicated with "h." This demonstrates clearly that the former interpretation [5] of the weak shoulder at the high-energy side as a $v''=1 \to v'=0$ transition is not correct. Instead we assign the shoulder consisting of the weak $3d\pi_{1/2}^{-1} \to {}^3\Sigma^-$ transition *and* vibrational lifetime interference contributions of the $3d\delta_{3/2}^{-1} \to {}^3\Sigma^-$ transition. Fit analyses neglecting vibrational lifetime interference were generally slightly worse, especially in the region indicated with L (Fig. 6). From this it can be concluded that it is necessary to include vibrational lifetime interference to explain the given spectra in detail. This holds as well for vibrationally resolved Auger spectra in other molecules. As, for example, displayed in Fig. 7, in HCl (DCl) a weak spectral feature, which is found to be $\cong 250$ meV ($\cong 200$ meV) above the Cl $2p_{1/2}^{-1} v''=0 \to {}^3\Sigma^- v'=0$ transi-
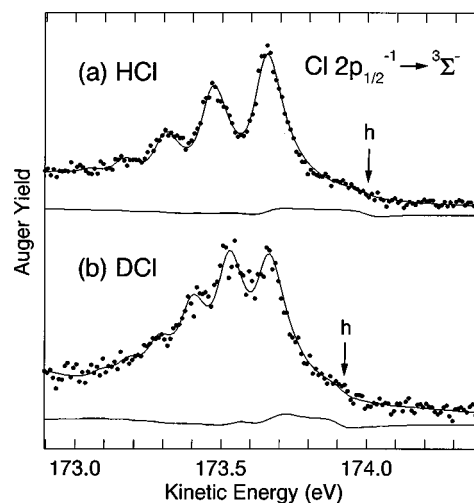
FIG. 7. The Cl $2p_{1/2}^{-1} \to {}^3\Sigma^-$ normal-Auger spectra of HCl and DCl. The solid line through the data points represent the fitted result and the solid subspectrum, the contributions of the vibrational lifetime interference. The vertical arrows indicate the expected energies for the Cl $2p_{1/2}^{-1} v''=1 \to {}^3\Sigma^- v'=0$ transitions based on the fitted result.

tion, has been assigned to a $v''=1 \to v'=0$ transition [4]. Considering the vibrational energy of 370 meV for HCl in the electronic ground state and the absence of higher vibrational states in the Cl $2p^{-1}$ photoelectron spectrum, i.e., a small change in the equilibrium distance [24]; it can directly be concluded that the vibrational energy of the core-excited state has to be close to the ground-state value. Therefore, the discussed spectral feature in HCl/DCl has to be reassigned as vibrational lifetime interference contributions. Contrary to the Cl $2p$ photoelectron spectra [24], the sign of the change in the equilibrium distance upon Cl $2p^{-1}$ ionization can be determined from the observed line shape of the

$$\langle f|n\rangle\langle n|i\rangle\langle i|m\rangle\langle m|f\rangle = \langle 0|0\rangle\langle 0|0\rangle\langle 0|1\rangle\langle 1|0\rangle$$

lifetime interference term: the equilibrium distance of the Cl $2p^{-1}$ core-ionized state of HCl/DCl is slightly larger than in the ground state. This conclusion is possible due to the fact that only the $\langle n|i\rangle = \langle 1|0\rangle$ matrix element depends on the sign of the change in the equilibrium distance upon core ionization. The Cl $2p_{1/2}^{-1} \to {}^3\Sigma^-$ Auger spectra of HCl and DCl given in Ref. [24] were reanalyzed by exploiting the present method, i.e., using the equilibrium distance and the vibrational energy of the Cl $2p_{1/2}^{-1}$ core-hole state as fit parameters. The result of the fit analysis is given by the solid lines through the data points in Fig. 7. The solid subspectra display the influence of the vibrational lifetime interference terms. The analysis indicates an increase of the equilibrium distance from $r''=1.275$ Å in the ground state to $r'=1.297(4)$ Å in the Cl $2p_{1/2}^{-1}$ core-hole state. This increase of the equilibrium distance $\Delta r = r' - r'' = 0.022(4)$ Å agrees reasonably well with calculations by Ellingson *et al.* [25] who obtained $\Delta r = 0.0236$ Å. For HCl (DCl) a decrease of the vibrational energy from $\hbar\omega''=370.4$ meV ($\hbar\omega''=259.4$ meV) in the ground state to $\hbar\omega'=357(5)$ meV [$\hbar\omega'=250(5)$ meV] in the core-ionized state was derived. For the two-hole final state $^3\Sigma^-$ an equilibrium distance of $r=$

1.452(5) Å and a vibrational energy $\hbar\omega=209(5)$ meV [$\hbar\omega=146(5)$ meV] for HCl (DCl) were obtained. These experimental values agree well with the theoretical results by Banichevich *et al.* [26] ($r=1.46$ Å, $\hbar\omega=217$ meV) and the experimental results obtained from the L_3VV Auger spectra by Svensson *et al.* [27] ($r=1.44$ Å, $\hbar\omega=226$ meV). The agreement with the equilibrium distance obtained by McConkey *et al.* [28] using threshold photoelectron coincidence spectroscopy is significantly worse ($r=1.39$ Å, $\hbar\omega=196$ meV). However, McConkey *et al.* [28] pointed out that their fit result for the $^3\Sigma^-$ state was unsatisfactory. They assumed indirect mechanisms to play a significant role in the population of the vibrational levels leading to incorrect results.

Although the spectra in Fig. 7 possess only moderate signal-to-noise ratios leading to fitted results with relatively large errors, the performed analysis clearly demonstrates that a normal-Auger spectrum contains detailed information not only about the final states but about the intermediate states as well.

V. SUMMARY AND CONCLUSION

We have presented a powerful method to understand the complex normal-Auger spectra including ligand-field splitting, vibrational splitting, and vibrational lifetime interference by describing all $3d^{-1}\rightarrow4p\pi^{-2}$ features in HBr and DBr simultaneously with approximately 30 free parameters. Considering the approximations used, the agreement between experimental spectra and fitted result is remarkably good. This method can be applied to different problems: By applying it to normal-Auger spectra with less overlapping transitions (e.g., HCl/DCl and HI/DI) under conditions where the PCI effect and non-Franck-Condon behavior of the intermediate state can be neglected, it can be used to study (i) the change in the geometry between the ground and the core-excited state and (ii) effects beyond the presented analysis. In (i) the high sensitivity of the lifetime-interference term can be exploited. This term only includes the overlap of the vibrational wave functions between the ground and the intermediate state instead of the squares of it. As a consequence, this term is more sensitive to small changes in the equilibrium geometry between the ground and intermediate states than the direct terms, which can be obtained from photoelectron spectroscopy. This application was demonstrated for the Cl $2p_{1/2}^{-1}\rightarrow{}^3\Sigma^-$ normal-Auger transition in HCl and DCl. The effects beyond the presented analysis (ii) include influences of lifetime and vibrational structure according to the deviations of the potential energy surfaces of the quasistable final states from the assumed Morse potential as well as electronic-state lifetime interference between different ligand-field components of the intermediate state. Up to now, electronic-state lifetime interference has only been studied in rare gas atoms [29,30]. (iii) The final states of resonant-Auger transitions measured under Raman conditions can often be described as nondissociative ionic two-hole configurations with one Rydberg electron in their field. The above-described method allows one to obtain information about the vibrational structure as well as about the geometry and vibrational energy of the two-hole state, which can be used to interpret the spectra.

[1] K. Siegbahn, C. Nordling, G. Johansson, J. Hedman, P. F. Hedén, K. Hamrin, U. Gelius, T. Bergmark, L. O. Werme, R. Manne, and Y. Baer, *ESCA Applied to Free Molecules* (North-Holland, Amsterdam, 1969).

[2] N. Correia, A. Flores-Riveros, H. Ågren, K. Helenelund, L. Asplund, and U. Gelius, J. Chem. Phys. **83**, 2035 (1985).

[3] T. X. Carroll, S. E. Andersson, L. Ungier, and T. D. Thomas, Phys. Rev. Lett. **58**, 867 (1987).

[4] L. Karlsson, P. Baltzer, S. Svensson, and B. Wannberg, Phys. Rev. Lett. **60**, 2473 (1988).

[5] W. Wannberg, S. Svensson, M. P. Keane, L. Karlsson, and P. Baltzer, Chem. Phys. **133**, 281 (1989).

[6] L. Karlsson, S. Svensson, P. Baltzer, M. Carlsson-Göthe, M. P. Keane, A. Naves de Brito, N. Correia, and B. Wannberg, J. Phys. B **22**, 3001 (1989).

[7] J. N. Cutler, G. M. Bancroft, and K. H. Tan, J. Phys. B **24**, 4987 (1991).

[8] Z. F. Liu, B. M. Bancroft, K. H. Tan, and M. Schachter, J. Electron Spectrosc. Relat. Phenom. **67**, 299 (1994).

[9] L. Karlsson, S. Svensson, P. Baltzer, A. Naves de Brito, N. Correia, and B. Wannberg, J. Phys. B **24**, L589 (1994).

[10] S. Aksela, A. Kivimäki, A. Naves de Brito, O.-P. Sairanen, S. Svensson, and J. Väyrynen, Rev. Sci. Instrum. **65**, 831 (1994).

[11] S. Aksela, A. Kivimäki, O.-P. Sairanen, A. Naves de Brito, E. Nõmmiste, and S. Svensson, Rev. Sci. Instrum. **66**, 1621 (1995).

[12] S. Svensson, J.-O. Forsell, H. Siegbahn, A. Ausmees, G. Bray, S. Södergren, S. Sundin, S. J. Osborne, S. Aksela, E. Nõmmiste, J. Jauhiainen, M. Jurvansuu, J. Karvonen, P. Barta, W. R. Salaneck, M. Evaldsson, M. Lögdlund, and A. Fahlman, Rev. Sci. Instrum. **67**, 2149 (1996).

[13] R. Püttner, M. Domke, K. Schulz, and G. Kaindl, J. Phys. B **28**, 2425 (1995).

[14] Y. F. Hu, Z. F. Liu, R. Püttner, G. M. Bancroft, and S. Aksela (unpublished).

[15] G. Herzberg, *Spectra of Diatomic Molecules* (Van Nostrand, Princeton, 1950), p. 534.

[16] M. Halmann and I. Laulich, J. Chem. Phys. **43**, 438 (1965).

[17] H. A. Ory, A. P. Gittleman, and J. P. Maddox, Astrophys. J. **139**, 346 (1964).

[18] G. B. Armen, J. Tulkki, T. Åberg, and B. Crasemann, Phys. Rev. A **36**, 5606 (1987).

[19] T. Matila, K. Ellingsen, T. Saue, H. Aksela, and O. Gropen (unpublished).

[20] H. Aksela, S. Aksela, H. Pulkkinen, G. M. Bancroft, and K. M. Tan, Phys. Rev. A **33**, 3876 (1986).

[21] S. Svensson, A. Ausmees, S. J. Osborne, G. Bray, F. Gel'mukhanov, H. Ågren, A. Naves de Brito, O.-P. Sairanen, A. Kivimäki, E. Nõmmiste, H. Aksela, and S. Aksela, Phys. Rev. Lett. **72**, 3021 (1994).

[22] J. Johnson, J. N. Cutler, G. M. Bancroft, Y. F. Hu, and K. H. Tan, J. Phys. B **30**, 4899 (1997).

[23] A. Banichevich, S. D. Peyerimhoff, B. A. Hess, and M. C. van Hemert, Chem. Phys. **154**, 199 (1991).

[24] H. Aksela, E. Kukk, S. Aksela, O.-P. Sairanen, A. Kivimäki, E. Nõmmiste, A. Ausmees, S. J. Osborne, and S. Svensson, J. Phys. B **28**, 4259 (1995).

[25] K. Ellingsen, T. Saue, H. Aksela, and O. Gropen, Phys. Rev. A **55**, 2743 (1997).

[26] A. Banichevich, S. D. Peyerimhoff, M. C. Van Hemert, and P. G. Fournier, Chem. Phys. **121**, 351 (1988).

[27] S. Svensson, L. Karlsson, P. Baltzer, M. P. Keane, and B. Wannberg, Phys. Rev. A **40**, 4369 (1989).

[28] A. G. McConkey, G. Dawber, L. Avaldi, M. A. MacDonald, G. C. King, and R. I. Hall, J. Phys. B **27**, 271 (1994).

[29] J.-E. Rubensson, M. Neeb, A. Bringer, M. Biermann, and W. Eberhardt, Chem. Phys. Lett. **257**, 447 (1996).

[30] E. Kukk, H. Aksela, A. Kivimäki, J. Jauhiainen, E. Nõmmiste, and S. Aksela, Phys. Rev. A **56**, 1481 (1997).